CHAPTER 4

On exo-cyclic aromaticity

4.1.

INTRODUCTION

Unambiguous definition of aromaticity has long been a subject of interest. Aromatic nature is correlated with a varietyof structural and energetic characteristics, such as highly symmetric structure, delocalized electrons, enhanced thermodynamic stability, reduced reactivity as compared to nonaromatic compounds and so on.[1-4] Other prominent indication of aromatic character comes from the properties like down-field shift in proton NMR peak positions resulting from the exaltation of diamagnetic susceptibility.[5,6] However, even after two centuries of existence,[7,8] still there is a scope of defining aromaticity unequivocally,[9] as understood from two legendary examples of complementary topological definition of aromaticity by Hückel[10] and Möbius.[11] The proposition by Hückel that cyclic-planar (4n+2) π-electron characterizes aromatic compounds is taken as gospel by the chemists.[10] Archetypal aromatic molecules contain a planar ring framework with equalized bond lengths. Though, Hückel's (4n+2) π rule is the easiest test to recognize aromaticity, its multidimensional nature often stands in the way of precisely identifying aromatic systems.[12-15] This apparently simple electron count rule was renewed by Dewar's insight of the tropolone structure.[16] In 1922 Crocker noticed that "aromatic structure is observed only in those combinations of elements which furnish six extra or aromatic electrons above those needed to complete a single-bonded ring" and described accurately the "six aromatic electron" structure[17] of benzene, pyridine, and five-membered ring heteroaromatics, earlier than the famous "aromatic sextet" paper by Armit and Robinson.[18]

4.2.

COMPUTATIONAL DETAILS

The minimum energy search was performed in Gaussian 09W suit of software at different DFT and *ab initio* methodologies.[19] ADF program[20] is also used for energy decomposition analysis (EDA) based on the methods of Ziegler and Rauk.[21] The total binding energy ΔE released upon the formation of the molecule from atomic fragments is divided into two major components, namely, ΔE_{prep} and ΔE_{int}, *i.e.*, $\Delta E = \Delta E_{prep} + \Delta E_{int}$. ΔE_{prep} corresponds

to the energy needed to promote the separated fragments from their equilibrium geometry to the final structure in the molecule. The interaction energy ΔE_{int} between the fragments is further decomposed into three physically meaningful terms, $\Delta E_{int} = \Delta E_{elstat} + \Delta E_{Pauli} + \Delta E_{orb}$. Here, ΔE_{elstat} is the classical electrostatic interaction between the promoted fragments as they are brought to their positions in the final complex. ΔE_{Pauli} corresponds to the repulsive Pauli interaction between occupied orbitals on the two fragments in the molecule. ΔE_{orb} represents interactions between the occupied molecular orbitals of one fragment with the unoccupied molecular orbitals of the other fragment and also signifies the mixing of occupied and virtual orbitals within the same fragment.[21] Diradical character y_i was estimated by means of PUHF method with the formula $y_i = 1 - {2T_i}/{1+T_i^2}$. The diradical character is defined by the weight of the doubly excited configuration in multiconfigurational self consistent field (MCSCF) theory and formally expressed by the overlap (T_i) between localized natural orbitals [highest occupied MO (HOMO) − i and lowest unoccupied MO (LUMO) + i], i being the number of MOs.[22] The dissected canonical molecular orbital NICS (CMO-NICS)[23,24] computation is performed using the ADF package. AdNDP is a compact combination of intuitive simplicity of Lewis theory with the flexibility and generality of Canonical Molecular Orbital theory thus providing a perfect description of systems featuring both localized and delocalized bonding without invoking the concept of resonance. AdNDP orbitals are analyzed using Multiwfn−A Multifunctional Wave function Analysis.[25] Molecular dynamics simulations were carried out with CP2K/Quickstep[26] package, which consists Born-Oppenheimer MD (BOMD) BLYP[27,28] GTH pseudopotentials[29,30] with a combined Plane-Wave (280 Ry density cutoff) and TZV2P basis sets.

4.2.1. Calculation of Ring Strain Energy (RSE)

The ring strain energy can be calculated with the help of Bader's Quantum theory of Atoms in Molecules (QTAIM).[31] The kinetic energy density at the ring critical point (3,+1) can be utilized to estimate the ring strain energy.[32] For the calculation of the RSE a regression equation, RSE=337.72×G(r)−8.115, is used as described in Ref. 20. The calculated RSE is found to be 27.98 kcal/mol.

4.2.2. Calculation of Aromatic Stabilization Energy:

The aromaticity of the proposed molecule is deemed to contribute significantly to its inherent stability. Recently, the stabilization in the molecular energy due to electronic mobility has been equated with the aromatic stabilization energy in the frame of second order perturbation theory. The proposed theoretical framework makes use of the inter-site hopping integral (t_{ij}) and the onsite repulsion energy (U) to account for the electron delocalization. The electronic population engaged in delocalization is obtained as a product of spin – orbital population ($n_{i\sigma}$ and $n_{j\sigma'}$) within the unrestricted framework and the degree of delocalization, which is estimated from electron localization function (ELF).

$$\Delta E = \sum_{i,j} \frac{t_{ij}^2}{U} \left(n_{i\sigma} n_{j\sigma'} + n_{i\sigma'} n_{j\sigma}\right) ELF^2 \tag{4.1}$$

However, the above equation had been derived for standard aromatic molecules which differ significantly from the present system with respect to the electronic structure and type of aromaticity. Particularly, the itinerancy of the lone pair of electrons in between the boron and fluorine completes the loop of electronic circulation and thus makes the pattern of electron delocalization unique with respect to traditional aromatic systems. To comply with this picture of electron delocalization, the above equation is split into two parts as follows,

$$\Delta E = \sum_{C,B} \frac{t_{ij}^2}{U} (n_{C\sigma} n_{B\sigma'} + n_{C\sigma'} n_{B\sigma}) ELF^2 + \sum_{F,B} \frac{2t_{ij}^2}{U} (n_{F\sigma} n_{B\sigma'} + n_{F\sigma'} n_{B\sigma}) ELF^2 \tag{4.2}$$

Here, the first part accounts for the electron delocalization within C – B ring, and the second part quantifies stabilization for electron delocalization within Lewis acid-base pair. The probability of both spin transfer from F to B is included by multiplying the stabilization term by two.

4.3.

RESULTS AND DISCUSSION

Aromatic cross-conjugated systems make it apparent that aromaticity must not be restricted only to the completely conjugated cyclic circuits.[33] This inspires us to study a four membered heteroatomic cyclic $C_2B_2F_4$ molecule with D_{2h} symmetry (Figure 4.1). Optimization of this molecule at different level of theory including coupled cluster singles double leads to a planar molecule (Dihedral angle 0.00°, Table 1 which is in agreement with the conclusions drawn in a recent report.[34] Geometry optimization is carried out from two different starting geometries, namely, rectangular and non-planar, to explore the possible existence of any isomer, specifically bond-stretch isomer,[35-37] of the present molecule. The convergence steps along with the energy of the final geometries from two different starting points suggest that both optimizations converge to the same structure depicting a planar as well as square C_2B_2 core (Figure 4.2).

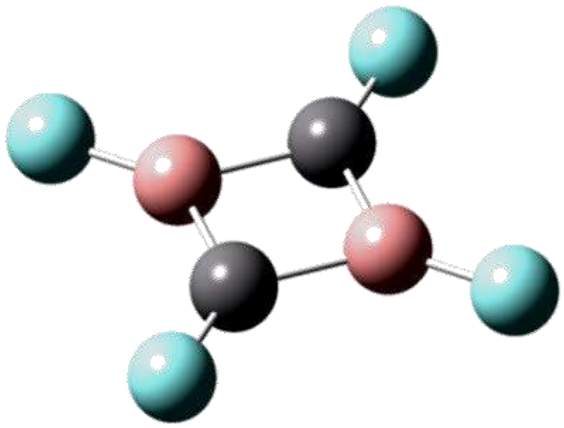

Figure 4.1. Optimized structure of $C_2B_2F_4$ cluster is of D_{2h} symmetry. The gray, pink and cyan spheres represent carbon, boron and fluorine atoms respectively.

Table 4.1. The optimized bond lengths (in Å) at different DFT and *ab initio* methodologies using aug-cc-pVDZ basis set.

Methodology (along with aug-cc-pVDZ basis set)	B-C bond length (in Å)	B-F bond length (in Å)	C-F bond length (in Å)	∠BCB bond angle (in °)	∠CBC bond angle (in °)	∠CBBC dihedral angle (in °)	Energy (in A.U.)	Minimum vibrational frequency (in cm^{-1})
QCISD*	1.542	1.340	1.319	93.23	86.77	0.00	−524.09	58.58
CISD*	1.527	1.330	1.303	93.18	86.82	0.00	−524.07	52.36
CCSD*	1.541	1.338	1.317	93.22	86.78	0.00	−524.09	57.82
MP2	1.544	1.350	1.331	93.86	86.14	0.00	−524.18	56.54
B3LYP	1.532	1.339	1.322	93.42	86.58	0.00	−525.40	61.90
B3PW91	1.531	1.337	1.317	93.48	86.52	0.00	−525.19	58.27
PBEPBE	1.541	1.347	1.331	93.54	86.46	0.00	−524.86	60.36
BLYP	1.543	1.350	1.340	93.57	86.43	0.00	−525.33	65.22
TPSSH	1.534	1.342	1.326	93.52	86.47	0.00	−525.41	61.65
CAM-B3LYP	1.525	1.334	1.315	93.44	86.56	0.00	−525.23	57.91
M-06	1.526	1.329	1.310	93.42	86.58	0.00	−525.19	60.51

*Computed with cc-pVDZ basis set

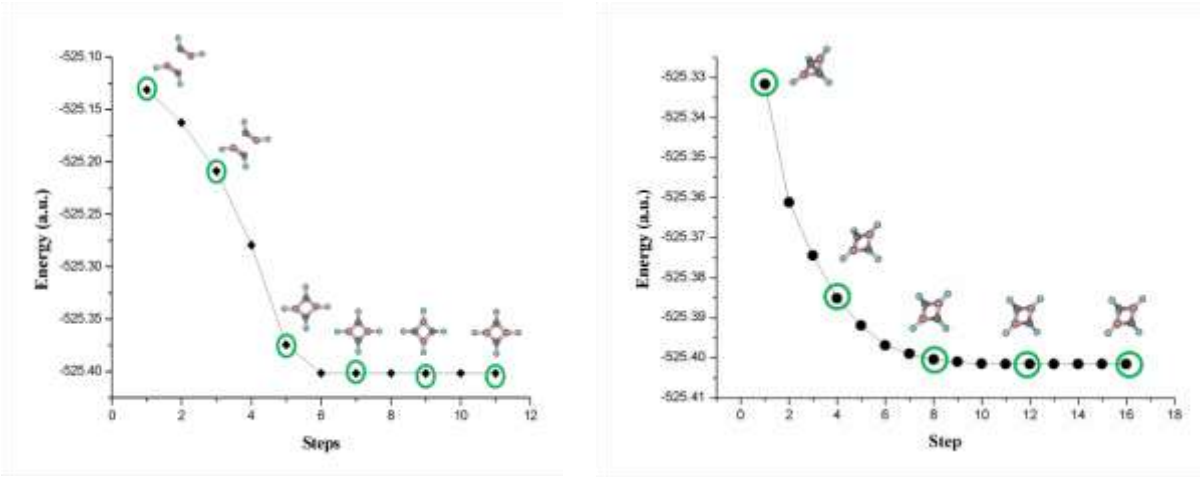

(a) (b)

Final Energy= −525.40156 a.u. **Final Energy**= −525.40156 a.u.

Figure 4.2. Geometry convergence during optimization of $C_2B_2F_4$ from (a) rectangular and (b) non-planar starting geometries and their corresponding final energies at B3LYP/aug-cc-pVDZ level. The points for which the geometries are presented in the plot are circled in green.

The dynamical stability of the molecule is confirmed from the absence of imaginary vibrational frequency (Table 4.1 and also by Molecular dynamics (MD) simulation. No sign of deformation is noted within 5 ps duration in the MD simulation at 300 K (see Figures 4.3, 4.4 and 4.5). The structural stability is often established from the binding energy of the molecule from individual atomic fragments. The larger the value of total binding energy, the more stable is the system. A large total binding energy (−1290.49 kcal/mol) thus advocates for the structural integrity of the system. The total binding energy is decomposed into two major components, namely, ΔE_{prep} and ΔE_{int}, i.e., $\Delta E = \Delta E_{prep} + \Delta E_{int}$, for convenience and ΔE_{int} is further decomposed into three physically meaningful terms, $\Delta E_{int} = \Delta E_{elstat} + \Delta E_{Pauli} + \Delta E_{orb}$. The structural and energy decomposition parameters computed at the B3LYP/aug-cc-pVDZ level are reported in Table 4.2. The reasonably high negative value of the total interaction energy (ΔE_{int}) is also signifies high stability of the molecule. Moreover, the ring strain energy value mentioned in the computational section is also in the range of reportedly stable four membered carbocyles and indicates structural stability. Followed by the validation of structural stability, the internal stability of the wave function is also confirmed with STABLE=OPT keyword implemented in Gaussian 09W.[38] The stable closed-shell electronic structure of the molecule is also indicated by negligibly small diradical character, y_i of

0.006.The closed-shell nature of the molecule is further substantiated by the large HOMO-LUMO gap of 5.2 eV.[39] Hence, the criteria of chemical viability proposed by Hoffmann et al. are persuasively satisfied.[40]

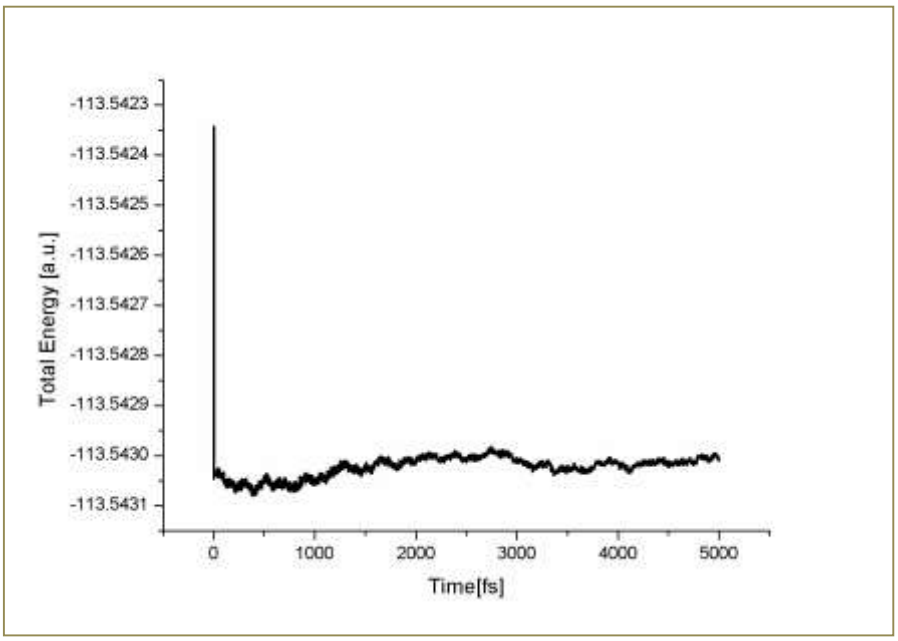

Figure 4.3. Variation of total energy of $C_2B_2F_4$ at T = 300 K along a DFT-based molecular dynamics simulation of 5 ps.

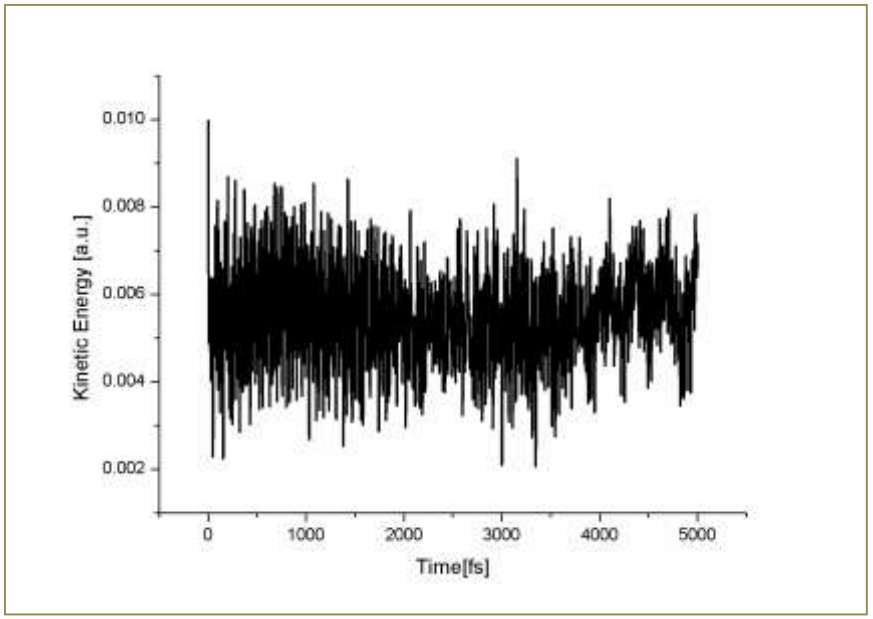

Figure 4.4. Variation of kinetic energy of $C_2B_2F_4$ at T = 300 K along a DFT-based molecular dynamics simulation of 5 ps.

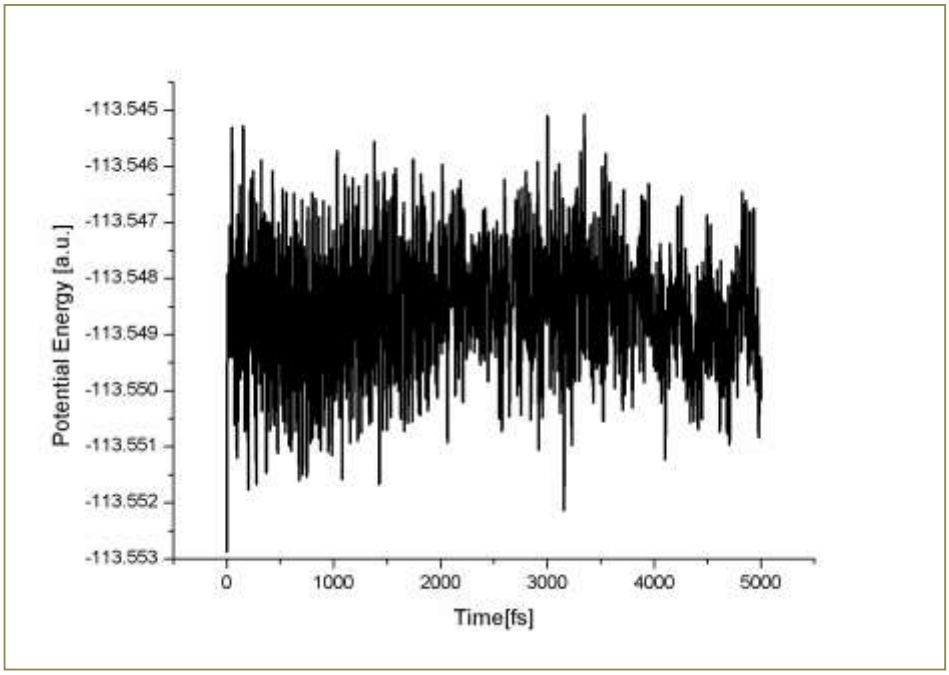

Figure 4.5. Variation of potential energy of $C_2B_2F_4$ at T = 300 K along a DFT-based molecular dynamics simulation of 5 ps.

Table 4.2. Summary of structural and energy decomposition parameters of $C_2B_2F_4$ computed at B3LYP/aug-cc-pVDZ level.

Parameters	Computed Values
B-C bond length (Å)	**1.532**
B-F bond length (Å)	**1.339**
C-F bond length (Å)	**1.322**
ΔE_{Pauli} (kcal/mol)	**1812.90**
ΔE_{elstat} (kcal/mol)	**−488.57**
ΔE_{orb} (kcal/mol)	**−1699.05**
ΔE_{int}(=ΔE_{Pauli} +ΔE_{elstat} +ΔE_{orb}) (kcal/mol)	**−374.72**

Satisfactory stability of the ring structure in $C_2B_2F_4$ stimulates to probe the possibility of cyclic electronic delocalization leading to aromaticity. Nucleus-independent chemical shift (NICS) is often considered as one of the superlative descriptors of aromaticity and is computed in terms of isotropic shielding tensor on a dummy atom in GIAO (Gauge Independent Atomic Orbitals) method.[41] A system is defined as aromatic (antiaromatic) based on the negative (positive) sign of the shielding tensor values, implying the presence of a diatropic (paratropic) ring current.[13] To find out the contribution of σ and π electrons to aromaticity, NICS has been calculated both in the center of the ring [NICS (0)], and at 1 Å above the plane [NICS(1)]. The negative values of NICS (0) and NICS (1), computed at different levels of theory (Table 4.3) provides strong indication in favour of the aromatic nature of $C_2B_2F_4$. Dissected canonical molecular orbital NICS (CMO-NICS) analysis is performed to identify orbitals with maximal contribution to NICS and hence to aromaticity. The orbitals that render significant diamagnetic contribution to the total NICS(1), which is found to be −6.33, are presented in Figure 4.6. The CMO-NICS(1) analysis (Figure 4.6) reveals strongest diatropic contribution of the lowest occupied π-orbital (HOMO−10) towards the NICS(1) value compared to modest contribution from higher π-orbitals (HOMO-6 & HOMO). Nevertheless, larger value of NICS(1) compared to NICS(0) suggests a major contribution of π-electrons towards aromaticity. In a recent work, the energy stabilization due to delocalization of π-electron is equated with aromatic stabilization energy (ASE) in the frame of second order perturbation theory.[42] The ASE is found to be 10.84 kcal/mol, which also suggests a substantial stabilization due to aromaticity. Visualization of the induced current density has been proved to be a useful tool for the study of aromaticity.[43] The vector plot of current density for the present molecule (Figure 4.7) exhibits the diatropic ring current for both π- and σ- planes illustrating the aromatic nature of the molecule. The peculiarity of π-electron flow gives rise to ring currents of adaxial-abaxial-adaxial pattern, as visualized in the current density vector map (Figure 4.7).

Table 4.3. The nucleus-independent chemical shift (NICS) values (ppm) in the ring plane [NICS (0)] and 1 Å above the ring plane [NICS (1)] at different DFT and *ab initio* methodologies using aug-cc-pVDZ basis set.

Methodology (along with aug-cc-pVDZ basis set)	NICS (0)	NICS (1)
B3LYP	−5.1673	−7.0986
B3PW91	−4.8444	−7.0370
PBEPBE	−3.3913	−6.2099
BLYP	−3.9376	−6.3329
CAM-B3LYP	−5.5683	−7.3992

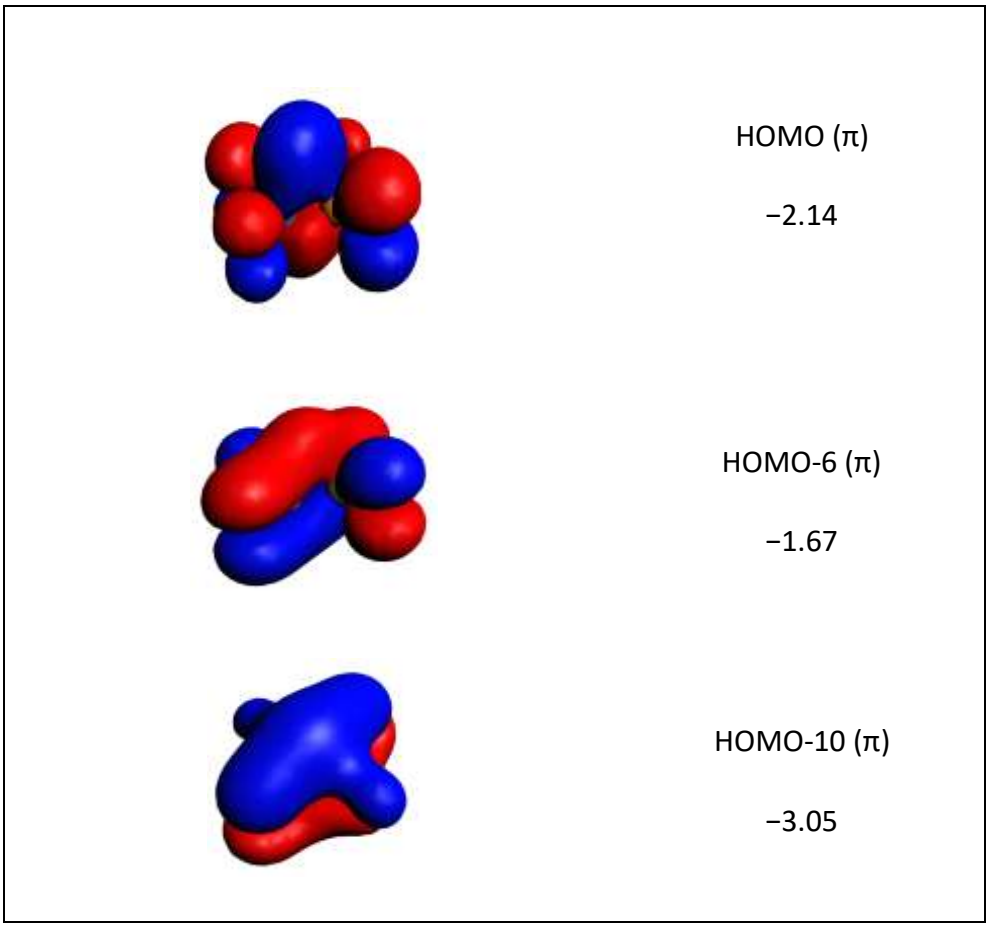

Figure 4.6. CMO-NICS analysis at 1 Å above the ring center of the $C_2B_2F_4$ molecule (D_{2h}).

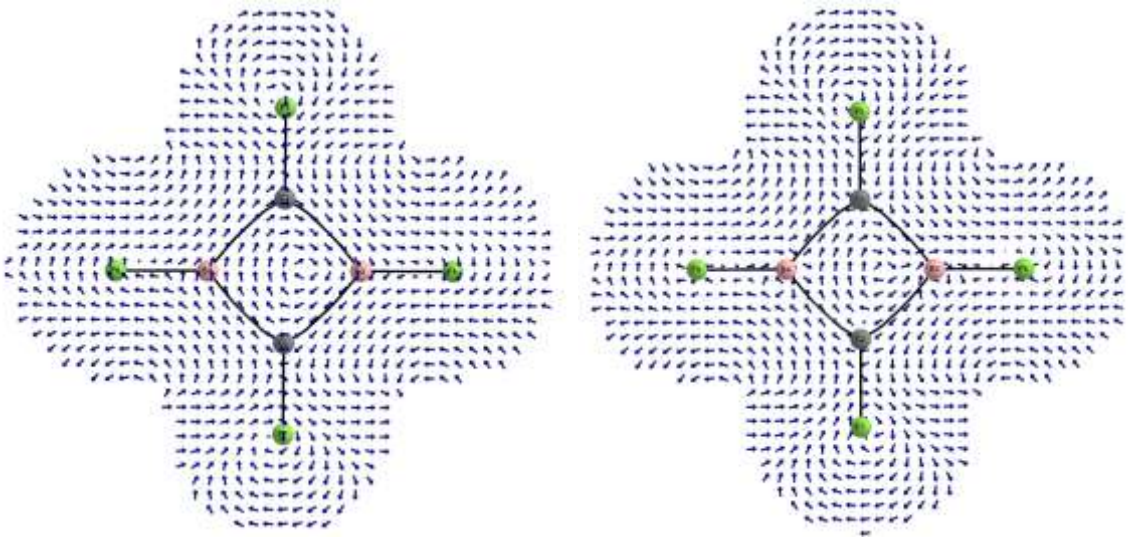

(a) (b)

Figure 4.7. The π- (a) and σ- (b) current density vector plots.

A very interesting fact that shows up in the CMO-NICS analysis is that the MO (HOMO-10 in Figure 4.6) which has the largest contribution towards NICS(1) includes F atoms as a major component. This indicates the involvement of B←F back-donated electrons to the aromatic π-cloud above and below the molecular plane. With these points, we infer that the molecular system is aromatic consisting of six π-electrons. Out of these six π-electrons, two electrons are from the p_z-orbitals of the sp^2 hybridized carbon atoms and the other four electrons are obtained through back-donation of paired electrons from fluorine to locally electron-deficient boron (Figure 4.8). Moreover, the ring current map (Figure 4.7) sustains the present model by displaying the π-density to be extended beyond the parent C_2B_2 ring up to the two B←F units in the molecule.

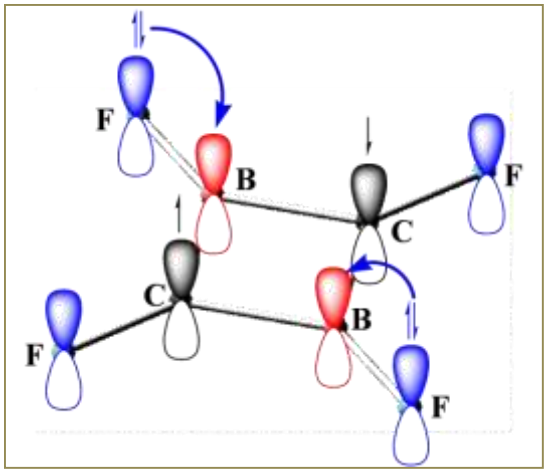

Figure 4.8. Orbital diagram for six π-electrons in $C_2B_2F_4$. The blue arrows indicate the role of the B←F back-bonding electrons to the formation of the aromatic π-cloud.

The key evidence in favor of our model comes from the energy decomposition analysis based on the extended transition state method and natural orbital for chemical valence scheme (ETS-NOCV).[44,45] The difference density, portrayed in Figure 4.9, dictates the involvement of the π-electrons of fluorine attached to boron in forming the aromatic π -electron cloud between the core C_2B_2-ring. Other than the dominant deformation channels corresponding to sigma bond formation between the fragments, a significant stabilization of −100 kcal/mol comes from the channel illustrating the flow of bonding electron pair from fluorine to the vacant $2p_z$-atomic orbitals of boron atoms. It is also noticed from Table 1 that a significant contribution to ΔE_{int} comes from the orbital interaction energy which also supports the current model.

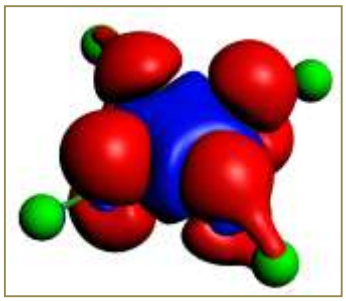

Figure 4.9. The ETS-NOCV difference density plot corresponding to −100 kcal/mol stabilization. The blue and red surfaces represent regions of the electron concentration and electron depletion (isosurface of 0.003 a.u.) respectively.

Adaptive Natural Density Partitioning (AdNDP)[46] is a new tool which can help to visualize the chemical bonding in a molecule in the most general way. AdNDP reveals the delocalized bonding elements related to the notion of aromaticity and antiaromaticity without taking the concept of resonance into account. Treating the electron pairs as the main element of chemical bonding, it models electronic structure of a molecule in terms of n-center-2-electron (nc-2e) bonds. Here, n spans in the interval from one to the total number of atoms in the molecule. Other than the Lewis bonding elements (1c-2e and 2c-2e, corresponding to the core electrons and lone pairs, and two-center two-electron bonds) it also picks up nc-2e delocalized bonding elements. The search for the all-center 2-electron bond in the molecule reveals an unambiguous description of aromaticity in $C_2B_2F_4$. The AdNDP orbital, portrayed in Figure 4.10, predicts the aromatic π-cloud to span fluorine atoms attached to the boron atoms extending the central C_2B_2-ring, thus showing exo-cyclic aromatic conjugation of π-electrons. This doubly occupied 6-centered-2-electron orbital portray the contribution of the said fluorine atoms to the aromatic character. Thus, this description of exo-cyclic aromaticity in the molecule is an extension beyond the classical concept of aromatic molecules with cyclic (4n+2) π conjugated system.

Occupation Number 1.99 Occupation Number 1.99

(a) (b)

Figure 4.10. The top-view of the AdNDP orbitals of $C_2B_2F_4$ (a) and $C_2B_2F_2H_2$ (b) along with their natural occupation numbers.

An *in silico* testing analogous systems with no back donation of 4 π-electrons to the empty $2p_z$-orbital of the boron atom stands necessary to establish the exo-cyclic nature of aromaticity in $C_2B_2F_4$. Thus, we chose to replace the F atoms attached to boron with hydrogen atoms. Harmonic frequency and NICS calculations are performed to judge the stability and aromaticity of the system. The minimum vibrational frequency 29.93 cm^{-1}, lies at a lower range, which evidently questions about its viability compared to $C_2B_2F_4$ at the first instance. Instability in this system also arises out of the σ-antiaromaticity as manifested by the positive values of NICS (0) (Table 4.4). Inspection of the results obtained from AdNDP calculation, performed for $C_2B_2F_2H_2$ reveals the involvement of only 2 π-electrons to the aromatic cloud which is centred only on the C_2B_2-core unlike $C_2B_2F_4$. This fact unambiguously proves the participation of the back donated π-electrons of p_z-orbitals from B←F in $C_2B_2F_4$. *In silico* tests are performed with $C_2B_2Cl_4$, $C_2B_2Br_4$ and $C_2B_2I_4$ systems to examine the effect of B←X back donation on the aromaticity of $C_2B_2X_4$ with X=F, Cl, Br and I. Harmonic frequency and NICS calculations are performed to assess their stability and aromaticity. The results are presented in Table S3. Low values of minimum vibrational frequencies make one sceptic about their viability at the first instance. Additionally the σ-antiaromaticity induces further instability of all these systems as is evident from the positive values of NICS (0). The $C_2B_2X_4$ systems show a decreasing trend in the NICS (1) value from fluorine to iodine (Table 4.4).

It is also to be noted that if B←X back donation is ignored, all the systems including $C_2B_2F_4$ at least posses 2 π-electrons which is capable to maintain the aromaticity in such systems. The AdNDP analyses clearly illustrate that there is no participation of back donated electrons to the aromatic electron cloud (Table 4.5). This observation substantiates the absence of back donation of π-electrons from higher p_z-orbitals of Cl ($3p_z$), Br ($4p_z$) and I ($5p_z$) to the empty $2p_z$-orbital of the boron atom due to energy mismatch. Instead, inspection of the AdNDP orbitals can establish the involvement of only 2 π-electrons to the aromatic cloud unlike $C_2B_2F_4$. The AdNDP analysis for $C_2B_2I_4$ could not be performed due to lack of similar basis set for iodine compared to other atoms.

Table 4.4. The optimized geometries, minimum harmonic frequencies, NICS (0) and NICS (1) values of $C_2B_2F_2H_2$, $C_2B_2Cl_4$, $C_2B_2Br_4$ and $C_2B_2I_4$ at B3LYP/aug-ccpVDZ level*.

Species	Minimum Frequency	NICS (0)	NICS (1)
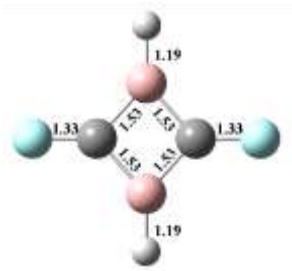	29.93	3.1873	−7.4007
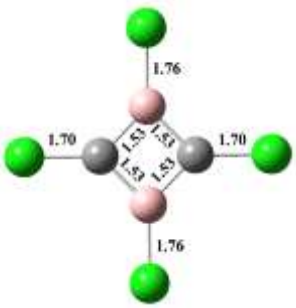	23.52	7.3817	−6.1710
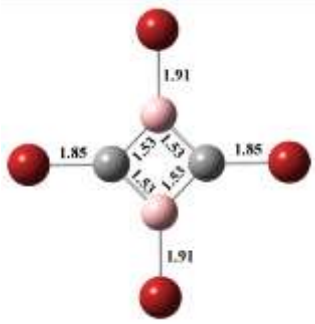	7.97	10.1049	−5.9335
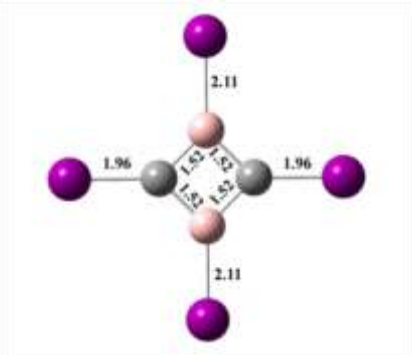	20.30	18.2129	−5.0623

*As the aug-cc-pVDZ basis set is not available for the element I, Sapporo-DKH3-DZP-2012 is applied as an extrabasis on I atoms.

Table 4.5. AdNDP orbitals along with occupations for the designed $C_2B_2Cl_4$ and $C_2B_2Br_4$ systems.

System	Occupation Number	AdNDP Orbital	
		Front View	Side View
$C_2B_2Cl_4$	1.99	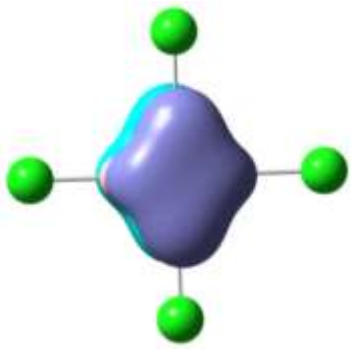	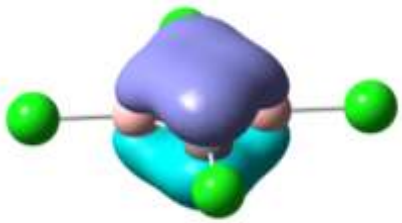
$C_2B_2Br_4$	2.00	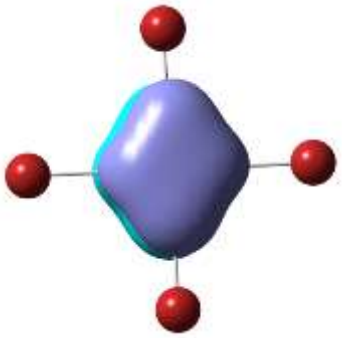	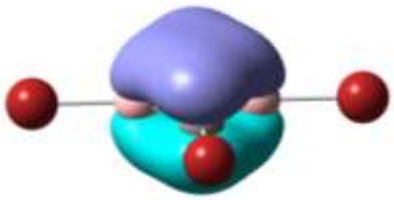

4.4.

CONCLUSIONS

In essence, the molecule $C_2B_2F_4$ acquires aromaticity due to unusual participation of exo-cyclic atoms. Back donation of 4 π-electrons from peripheral fluorine atoms to the electron-deficient boron atoms helps the ring to gain the magic number of 6 π-electrons leading to a unique exo-cyclic aromaticity. Moreover, the existence of molecule with similar C_2B_2 core (compound III/IV in ref. 47) makes us optimistic about the experimental realization of the molecule in near future.

4.5.

REFERENCES

1. Garratt, P. J. *Aromaticity*, John Wiley & Sons, 1986.
2. Minkin, V. I.; Glukhotsev, M. N.; Simkin, B. Y. in Aromaticity and Antiaromaticity: Electronic and Structural Aspects, John Wiley & Sons, Inc., New York, 1994.
3. Bickelhaupt, F.; de Wolf, W. H. *Recl. Trav. Chim. Pays-Bas* **1988**, *107*, 459-478.
4. Kraakman, P. A.; Valk, J.- M.; Niederländer, H. A. G.; Brouwer, D. B. E.; Bickelhaupt, F. M.; de Wolf, W. H.; Bickelhaupt F.; Stam, C. H. *J. Am. Chem. Soc.* **1990**, *112*, 6638-6646.
5. Schleyer P. v. R.; Jiao, H. *J. Pure Appl. Chem*. **1996**, *68*, 209-218.
6. Carey F. A.; Sundberg, R. J. *Advanced Organic Chemistry: Structure And Mechanisms (Part A)*, Springer, 2000.
7. Faraday, M. *Phil. Trans. R. Soc.* **1825**, *115*, 440–466.
8. Kekulé, A. *Bull. Soc. Chim.Fr.* **1865**, *3*, 98-110.
9. Balaban, A. T.; Schleyer P. v. R.; Rzepa, H. S. *Chem. Rev.* **2005**, *105*, 3436-3447.
10. Huckel, E. *Z. Phys.* **1931**, *70*, 204-286.
11. Heilbronner, E. *Tetrahedron Lett.* **1964**, *5*, 1923–1926.
12. Balaban, A. T. *Pure & Appl. Chem.* **1980**, *52*, 1409-1429.
13. Katrizky, A.; Barczymski, P.; Musumarra, G.; Pisano D.; Szafran, M. *J. Am. Chem. Soc.* **1989**, *111*, 7-15.
14. Schleyer, P. v. R.; Maerker, C.; Dransfeld, A.; Jiao, H.; Hommes, N. J. R. v. E. *J. Am. Chem. Soc.* **1996**, *118*, 6317-6318.
15. Misra, A.; Klein, D. J.; Morikawa, T. *J. Phys. Chem. A*, **2009**, *113*, 1151-1158.
16. Dewar, M. J. S. Tropolone. *Nature* **1950**, *166*, 790-791.
17. Crocker, E. C. *J. Am. Chem. Soc.*, **1922**, *44*, 1618-1630.
18. Armit, J. W.; Robinson, R. *J. Chem. Soc.* **1925**, *127*, 1604-1618.
19. Gaussian 09, Revision B.01, Frisch, M. J.; Trucks, G. W.; Schlegel, H. B.; Scuseria, G. E.; Robb, M. A.; Cheeseman, J. R.; Scalmani, G.; Barone, V.; Mennucci, B.; Petersson, G. A.; Nakatsuji, H.; Caricato, M.; Li, X.; Hratchian, H. P.; Izmaylov, A. F.; Bloino, J.; Zheng, G.; Sonnenberg, J. L.; Hada, M.; Ehara, M.; Toyota, K.; Fukuda, R.; Hasegawa, J.; Ishida, M.; Nakajima, T.; Honda, Y.; Kitao, O.; Nakai, H.; Vreven, T.; Montgomery, J. A., Jr.; Peralta, J. E.; Ogliaro, F.; Bearpark, M.; Heyd, J. J.; Brothers, E.; Kudin, K. N.; Staroverov, V. N.; Kobayashi, R.; Normand, J.; Raghavachari, K.; Rendell, A.; Burant, J. C.; Iyengar, S. S.; Tomasi, J.; Cossi, M.; Rega, N.; Millam, J. M.; Klene, M.; Knox, J. E.; Cross, J. B.; Bakken, V.; Adamo, C.; Jaramillo, J.; Gomperts, R.; Stratmann, R. E.; Yazyev, O.; Austin, A. J.; Cammi, R.; Pomelli, C.; Ochterski, J. W.; Martin, R. L.; Morokuma, K.; Zakrzewski, V. G.; Voth, G. A.; Salvador, P.; Dannenberg, J. J.; Dapprich, S.; Daniels, A. D.; Farkas, Ö.; Foresman, J. B.; Ortiz, J. V.; Cioslowski, J.; Fox, D. J. Gaussian, Inc., Wallingford CT, 2009.

20. Amsterdam Density Functional (Theoretical Chemistry, Vrije Universiteit, Amsterdam, The Netherlands, http://www.scm.com).
21. Ziegler, T.; Rauk, A. *Theor. Chim. Acta.* **1977**, *46*, 1-10.
22. Yamaguchi, K. *Self-Consistent Field: Theory and Applications.* (Eds Carbo, R., Klobukowski, M.); Elsevier: Amsterdam, 1990.
23. Corminboeuf, C.; Heine, T.; Weber, J. *Phys. Chem. Chem. Phys.* **2003**, *5*, 246-251.
24. Corminboeuf, C.; King, R. B.; Schleyer, P. v. R. *Chem. Phys. Chem.* **2007**, *8*, 391-398.
25. Lu, T.; Chen, F. *J. Comp. Chem.* **2012**, *33*, 580-592.
26. VandeVondelea, J.; Krackb, M.; Mohamedb, F.; Parrinellob, M.; Chassaingc, T.; Hutter, J. *Comput. Phys. Commun.* **2005**, *167*, 103-128.
27. Becke, A. D. *Phys. Rev. A* **1988**, *38*, 3098-3100.
28. Lee, C.; Yang, W.; Parr, R. G. *Phys. Rev. B* **1988**, *37*, 785-789.
29. Goedecker, S.; Teter, M.; Hutter, J. *Phys. Rev. B* **1996**, *54*, 1703-1710.
30. Hartwigsen, C.; Goedecker, S.; Hutter, J. *Phys. Rev. B* **1998**, *58*, 3641-3662.
31. Bader, R.F.W. *Atoms in Molecules: A Quantum Theory*; Oxford University Press: Oxford, UK, 1990.
32. Bauzá, A.; Quiñonero, D.; Deyà, P. M.; Frontera, A. *Chem. Phys. Lett.* **2012**, *536*, 165–169.
33. Gund, P. *J. Chem. Educ.* **1972**, *49*, 100-103.
34. McKee, W. C.; Wu, J. I.; Hofmann, M.; Berndt A.; Schleyer, P. v. R. *Org. Lett.*, **2012**, *14*, 5712–5715.
35. Goswami, T.; Paul, S.; Mandal, S.; Misra, A.; Anoop, A.; Chattaraj, P. K. *Int. J. Quantum Chem.*, **2015**, *115*, 426-433.
36. Giri, S.; Kumar, R. P. S. A.; Chakraborty A.; Roy, D. R.; Duley, S.; Parthasarathi, R.; Elango, M.; Vijayaraj, R.; Subramanian V.; Merino, G.; Chattaraj, P. K. in *Aromaticity and Metal Clusters*, CRC Press, USA, **2011**.
37. Chattaraj, P. K.; Das, R.; Duley, S.; Vigneresse, J. -L. *Theor. Chem. Acc.*, **2012**, *131*, 1089-1096.
38. Seeger, R.; Pople, J. A. *J. Chem. Phys.* **1977**, *66*, 3045-3050.
39. Dohnert, D.; Koutecky, J. *J. Am. Chem. Soc.*, **1980**, *102*, 1789-1796.
40. Hoffmann, R.; Schleyer, P. v. R.; Schaefer, H. F. *Angew. Chem., Int. Ed.* **2008**, *47*, 7164-7167.
41. Wolinski, K.; Hinton, J. F.; Pulay, P. *J. Am. Chem. Soc.*, **199**
42. Paul, S.; Goswami, T.; Misra, A. *AIP Adv.* **2015**, *5*, 107211.
43. Steiner, E.; Fowler, P. W.; Soncini, A.; Jenneskens, L. W. *Faraday Discuss.*, **2007**, *135*, 309–323.
44. Mitoraj, M.; Michalak, A. *J. Mol. Model.*, **2007**, 13, 347-355.
45. Mitoraj, M. P.; Michalak, A.; Ziegler, T. *J. Chem. Theory Comput.* **2009**, 5, 962-975.
46. Zubarev, D. Y.; Boldyrev, A. I. *Phys. Chem. Chem. Phys.* **2008**, *10*, 5207-5217
47. Bromm, D.; Stalke, D.; Heine, A.; Miller, A. *J. Organomet. Chem.*, **1990**, *386*, 1-7.